

Hot deformation characteristics and strain-dependent constitutive analysis of Inconel 600 superalloy

Horng-Yu Wu · Feng-Jun Zhu · Shang-Chih Wang ·
Woei-Ren Wang · Chien-Cheng Wang ·
Chui-Hung Chiu

Received: 18 September 2011 / Accepted: 3 January 2012 / Published online: 10 January 2012
© Springer Science+Business Media, LLC 2012

Abstract The hot deformation characteristics and constitutive analysis of Inconel (IN) 600 superalloy were investigated at elevated temperatures. Hot compressive tests were carried out in the temperature and strain rate ranging from 900 to 1150 °C and 1×10^{-3} – 10 s^{-1} , respectively. The flow behavior analyses and microstructural observations indicate that the softening mechanisms were related to dynamic recrystallization (DRX) and grain growth. DRX played a dominant role in the microstructural evolution at low temperatures (or high strain rates). DRX was the dominant softening effect at low strains on testing at high temperatures with low strain rates, whereas growth of the dynamically recrystallized grains was responsible for softening at high strains. The flow stress of IN 600 was fitted well by the constitutive equation of the hyperbolic sine function under the deformation conditions performed in this study. A constitutive equation as a function of strain was established through a simple extension of the hyperbolic sine constitutive relation.

Introduction

The Inconel (IN) 600 Ni-base superalloy combines excellent oxidation and corrosion resistance at high temperatures. IN 600 is widely used as a high-temperature material in the nuclear and aerospace industries, in which controlling the microstructure of the hot-worked component is required. During hot deformation, the dynamic softening process operates simultaneously with the deformation process. The softening process, such as dynamic recovery (DRV) and/or dynamic recrystallization (DRX), relaxes the hardening caused by the deformation process [1, 2]. The high-temperature mechanical properties of superalloys are highly sensitive to the flow characteristic and microstructural changes during hot working [3, 4]. Changes in the microstructure of an alloy also influence its deformation mechanism [5, 6], which is dependent on the deformation conditions, particularly temperature and strain rate. An understanding of the constitutive behavior of superalloys is essential in optimizing workability and controlling the microstructural evolution during hot working.

In describing the hot deformation behavior of a metal, the constitutive relationship among the flow stress, deformation temperature, and strain rate is generally expressed by the hyperbolic sine law [7–10]:

$$\dot{\epsilon} = A [\sinh(\alpha\sigma)]^n \exp\left[\frac{-Q}{RT}\right] \quad (1)$$

where A (s^{-1}) and α (MPa^{-1}) are constants, n is the stress exponent, Q is the activation energy, and σ is the steady state stress, peak stress, or the stress for a given strain.

Constitutive analysis has been carried out on a large number of alloys. Cai et al. [11] investigated the characteristics of the hot deformation behavior of a Ni-base superalloy based on the peak stress and found that the

H.-Y. Wu (✉) · F.-J. Zhu
Department of Mechanical Engineering, Chung Hua University,
Hsinchu 300, Taiwan
e-mail: ncuwu@chu.edu.tw

S.-C. Wang · W.-R. Wang · C.-C. Wang
Nanopowder and Thin Film Technology Center, ITRI South,
Industrial Technology Research Institute, Tainan 709, Taiwan

C.-H. Chiu
Material and Chemical Research Laboratories, Industrial
Technology Research Institute, Chutung 310, Taiwan

stress exponent n could be taken as a constant in the strain rate range of $0.001\text{--}1\text{ s}^{-1}$. Yuan and Liu [12] studied the effect of the δ phase on the hot deformation behavior of IN 718 using a hyperbolic sine equation to characterize the dependence of the peak stress on the deformation temperature and strain rate. Thomas et al. [13] explored the high-temperature deformation of IN 718 and showed that the n value, derived from the peak stress, does not depend on the temperatures greater than $900\text{ }^{\circ}\text{C}$. Jiang et al. [14] found that the relation of the peak stress with the strain rate and temperature satisfies the hyperbolic sine law for 8% Cr steel. Farnoush et al. [15] investigated the hot deformation characteristics of 2205 duplex stainless steel using the steady state flow stress.

In general, Eq. 1 relates the peak stress or steady state flow stress to the temperature and strain rate on the hot deformation test. However, the steady state may not be reached in deformation at high strain rates or low temperatures even at large strains [16–18]. According to Slooff et al. [16], the constitutive parameter A increases with the increasing strain for magnesium AZ series alloys. Strain is one of the major controlling parameters during the hot-forming process. Therefore, strain-dependent constitutive analysis is required to model the non-steady state deformation behavior in high-temperature deformation.

In this study, the hot compression tests of IN 600 were performed at various temperatures and strain rates. Based on the measured flow stress, hot deformation characteristics were analyzed, and a strain-dependent constitutive relationship was developed. The constitutive parameters obtained were validated by comparing the predicted flow stresses with the experimentally measured ones.

Experimental procedures

Table 1 shows the chemical composition of the IN 600 used in this study. The starting material was in the annealed condition. Figure 1 shows the as-received microstructure. Cylindrical specimens with a height of 9 mm and diameter of 6 mm were machined from the rod for the compression tests. Hot compressed tests were conducted on a Gleeble-3500 thermal simulation machine at temperatures ranging from 900 to $1150\text{ }^{\circ}\text{C}$ and at strain rates varying between 1×10^{-3} and 10 s^{-1} . Graphite foil was used as a lubricant between the specimen and the compression dies. Thermocouples were welded on the surface of the compression

specimen to measure temperature. Specimens were heated to the test temperature and maintained for 3 min before hot compression. The initial height of the specimen was reduced to approximately 50%, which corresponds to the true strain of approximately 0.7. Some specimens were compressed to the height corresponding to the true strains of approximately 0.2, 0.4, and 0.6, to examine the microstructural evolution during hot deformation. The specimens were water quenched immediately after hot compression. The flow stress data obtained at various temperatures and strain rates were corrected for the adiabatic temperature increase.

The specimens for microscopic examination were prepared using conventional metallographic techniques. The polished specimens were electrically etched in an etchant composed of 10% natal. An optical microscope was used to examine the microstructures.

Results and discussion

Flow behavior

Figure 2 illustrates the stress–strain curves obtained at temperatures of 900 and $1050\text{ }^{\circ}\text{C}$. The flow curves exhibit typical flow behavior with dynamic softening. The flow stress increases and reaches a peak value, after which the stress decreases with increasing strain. The steady state can be reached at low strain rates but not at high strain rates. The features of the flow curves for IN 600 alloy indicate the occurrence of DRX phenomenon during hot deformation [1, 2]. The rates of strain hardening and strain softening vary with deformation temperature and strain rate. At high strain rates, hardening followed by softening is more noticeable, whereas at low strain rates, a dynamic equilibrium between hardening and softening occurs at the very beginning of deformation. The initial rapid rise in stress is associated with an increase in dislocation density, as a result of strain hardening. At high strain rates, dislocation multiplication is more rapid than at low strain rates and contributes to higher strain hardening effect.

Figure 3 shows the variation in the peak stress as a function of temperature at various strain rates. The peak stress is evidently dependent on the strain rate and temperature. The stress decreases with decreasing strain rate at a fixed temperature. However, the extent of decrease depends on the temperature. The effect of the strain rate on

Table 1 Composition of IN 600 investigated

Element	C	Mn	Si	P	Cr	Fe	Ti	Ni
wt%	0.08	0.75	0.35	0.009	15.9	9.41	0.22	Bal.

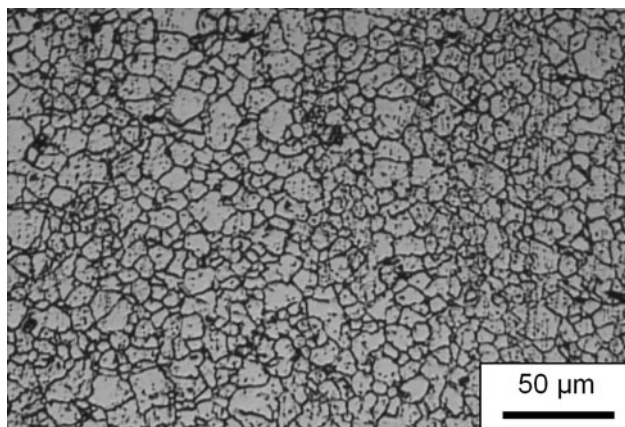


Fig. 1 Optical image of the initial microstructure of IN 600

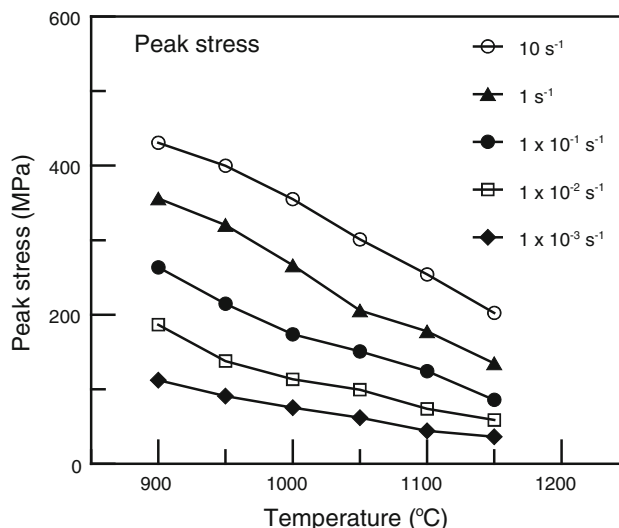


Fig. 3 Peak stress as a function of temperature at various strain rates

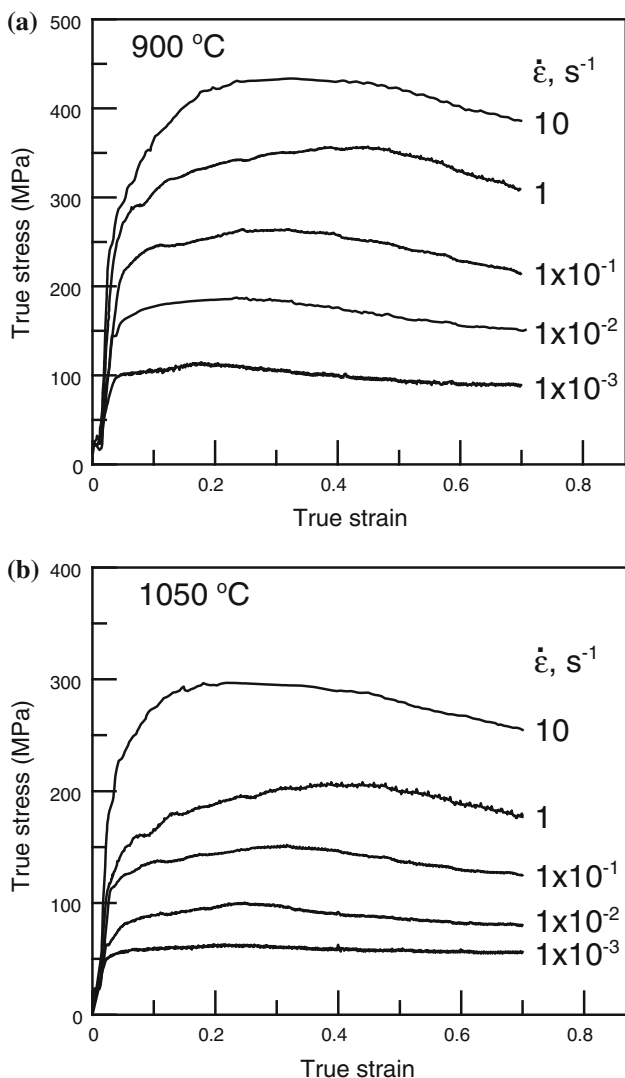


Fig. 2 Compression curves for the IN 600 specimens at various strain rates at a 900 °C and b 1050 °C

the peak stress is more pronounced at low temperatures. Moreover, peak stress increases with decreasing temperature at a given strain rate. The peak stress significantly decreases with increasing temperature at high strain rates. In contrast, the differences in the peak stress between different temperatures are smaller at low strain rates. Increasing strain rate at low temperatures leads to an increase in the dislocation density, resulting in higher-stress concentration regions. Therefore, peak stress increases noticeably with strain rate at low temperatures. Decreases in the peak stresses at low strain rate can be related to DRX whereby there is more time for nucleation and growth of DRX.

Constitutive analysis

Taking the natural logarithms of both sides of Eq. 1 yields the following:

$$\ln[\sinh(\alpha\sigma)] = \frac{1}{n} \ln \dot{\epsilon} + \frac{Q}{nR} \left(\frac{1}{T} \right) - \frac{1}{n} \ln A \tag{2}$$

The value of α may be chosen in a way that parallel lines are obtained from the curves of $\ln \dot{\epsilon}$ versus $\ln[\sinh(\alpha\sigma)]$. According to Eq. 2, n is the slope of the plot of $\ln \dot{\epsilon}$ versus $\ln[\sinh(\alpha\sigma)]$ at a given strain and temperature. The value of Q can be calculated using the slope of the plot of $\ln[\sinh(\alpha\sigma)]$ versus $1/T$ at a constant strain and strain rate.

Figure 4 shows the relationship between the logarithmic peak stress ($\ln[\sinh(\alpha\sigma_p)]$) and the logarithmic strain rate ($\ln \dot{\epsilon}$) at the temperature range of 900–1150 °C. The value of α , which has the best fit among the experimental data, is obtained as 0.005 MPa⁻¹. The average value of the stress exponent n is 4.7, with a maximum deviation of approximately 4.7%. Figure 5 presents the changes in peak stress

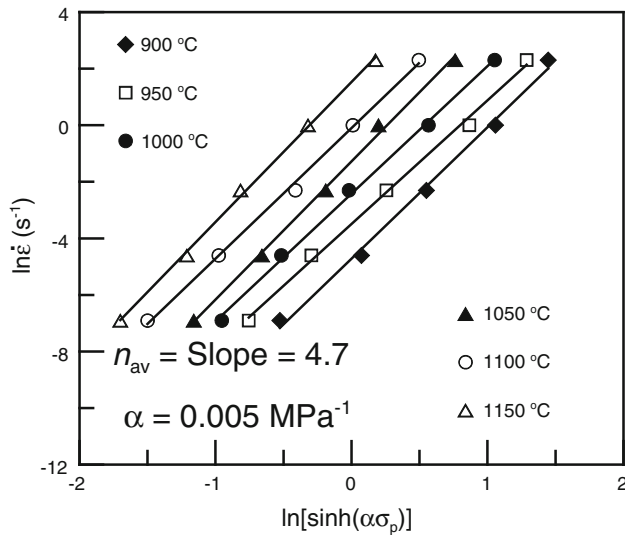


Fig. 4 Variation in $\ln \dot{\epsilon}$ as a function of $\ln[\sinh(\alpha\sigma_p)]$ at various temperatures

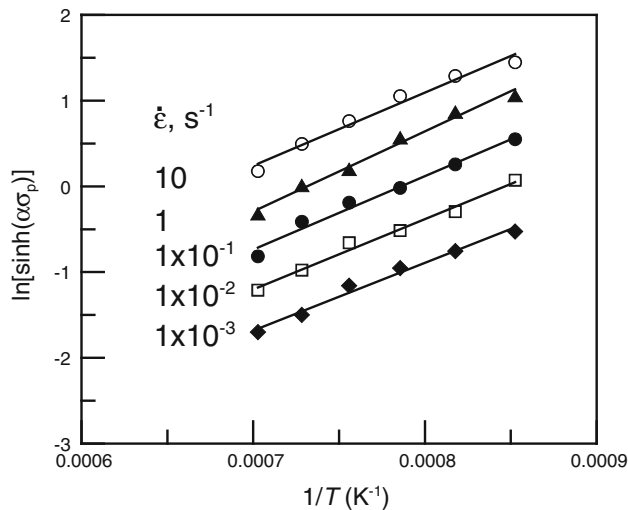


Fig. 5 Variation in $\ln[\sinh(\alpha\sigma_p)]$ as a function of reciprocal temperature at various strain rates

as a function of reciprocal temperature. The value of the activation energy Q calculated using the slopes of the plots in Figs. 4 and 5 is approximately 330 kJ/mol for IN 600. The Q value is higher than the value of 285 kJ/mol for self-diffusion in pure Ni [13], whereas the Q value is lower than the reported values of other Ni-base superalloys. The reported Q values are 379.28, 443.2, 449, and 380.215 kJ/mol for Nimonic 80A [19], IN 718 [20], Haynes230 [21], and IN 690 [3], respectively. The calculated Q value is approximately 13% lower than that for IN 690. Both IN 600 and IN 690 are Ni-base superalloys with Fe and Cr additions. The addition of Fe reduces the activation energy for Cr in Ni [22]. Cr leads to the formation of Cr_{23}C_6

intermetallic carbide in superalloys. In comparison with IN 600, IN 690 presents more carbide particles because of its higher Cr content. An alloy with a higher content of intermetallic particles raises the activation energy [23, 24]. Therefore, a lower activation energy Q value for IN600 is caused by a lower content of Cr.

The constitutive equation can be related to the Zener–Hollomon parameter Z [25], which is defined as follows:

$$Z = \dot{\epsilon} \exp\left[\frac{Q}{RT}\right] = A[\sinh(\alpha\sigma)]^n \quad (3)$$

Z combines the deformation variables strain rate and temperature through an Arrhenius function with the activation energy Q . Taking the natural logarithms of both sides of Eq. 3 yields the following:

$$\ln Z = \ln A + n \ln[\sinh(\alpha\sigma)] \quad (4)$$

Equation 4 indicates that a linear relation between $\ln[\sinh(\alpha\sigma)]$ and $\ln Z$ should exist. The relationship between $\ln Z$ and $\ln[\sinh(\alpha\sigma_p)]$ shown in Fig. 6 indicates that the relation of peak stress and temperature satisfies Eq. 4. The coefficient of determination R^2 of the fit is 0.99. By substituting the calculated parameters into Eq. 1, the constitutive equation for IN 600 based on the peak stress is expressed as:

$$\dot{\epsilon} = 3.95 \times 10^{12} [\sinh(0.05\sigma_p)]^{4.7} \exp\left[\frac{-330000}{RT}\right] \quad (5)$$

The peak stresses, as calculated using Eq. 5, are compared with the measured peak stresses, as shown in Fig. 7. Clearly, the calculated stresses match the measured stresses well. The constitutive equation obtained in this study gives reasonable fit to the measured values. This result indicates

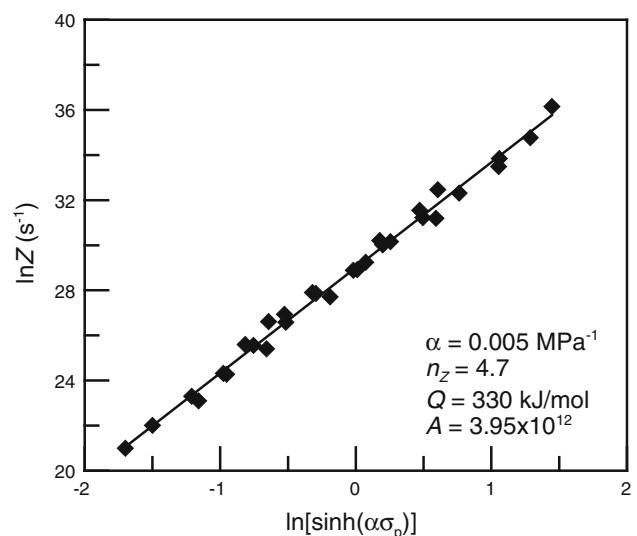


Fig. 6 Calculation of the Zener–Hollomon parameter of the hot compressed IN 600

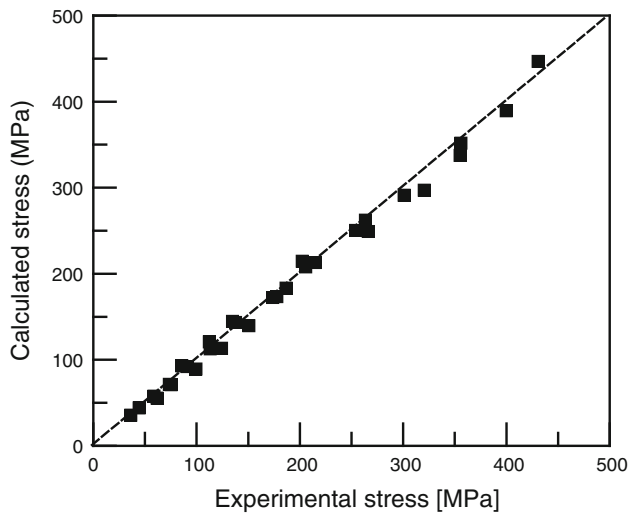


Fig. 7 Comparison between the calculated and the measured peak stresses for IN 600. The *dashed line* indicates a perfect match between the calculation and measurement

that the constitutive relationship among the flow stress, deformation temperature, and strain rate for IN 600 during hot deformation satisfies the hyperbolic sine law.

Microstructure analysis

Figure 8 shows the microstructures of the IN 600 specimens deformed under different conditions. The microstructures indicate that DRX occurs during hot compression. The grain size decreases with decreasing temperature (or increasing strain rate). The grain size depends sensitively on the deformation temperature and/or strain rate. These observations reveal that the microstructural behaviors are related to the Zener–Hollomon parameter Z . Table 2 shows the $\ln Z$ values, obtained from Eq. 3, under different deformation conditions. Figure 8 shows that the grain size decreases with increasing Z value. Increasing the Z value, that is, decreasing the deformation temperature or increasing the strain rate. A high Z value leads to a lower DRX kinetics because of lower diffusivity at lower temperatures and/or insufficient time at higher strain rates. As there is not enough time for diffusion to take place at high strain rates, therefore the grain growth is not so pronounced. The growth of the new grains is limited, thereby reducing the size of the dynamically recrystallized grains. Similar relationships were also observed in IN 718 [20] and AISI 304 austenitic stainless steel [26].

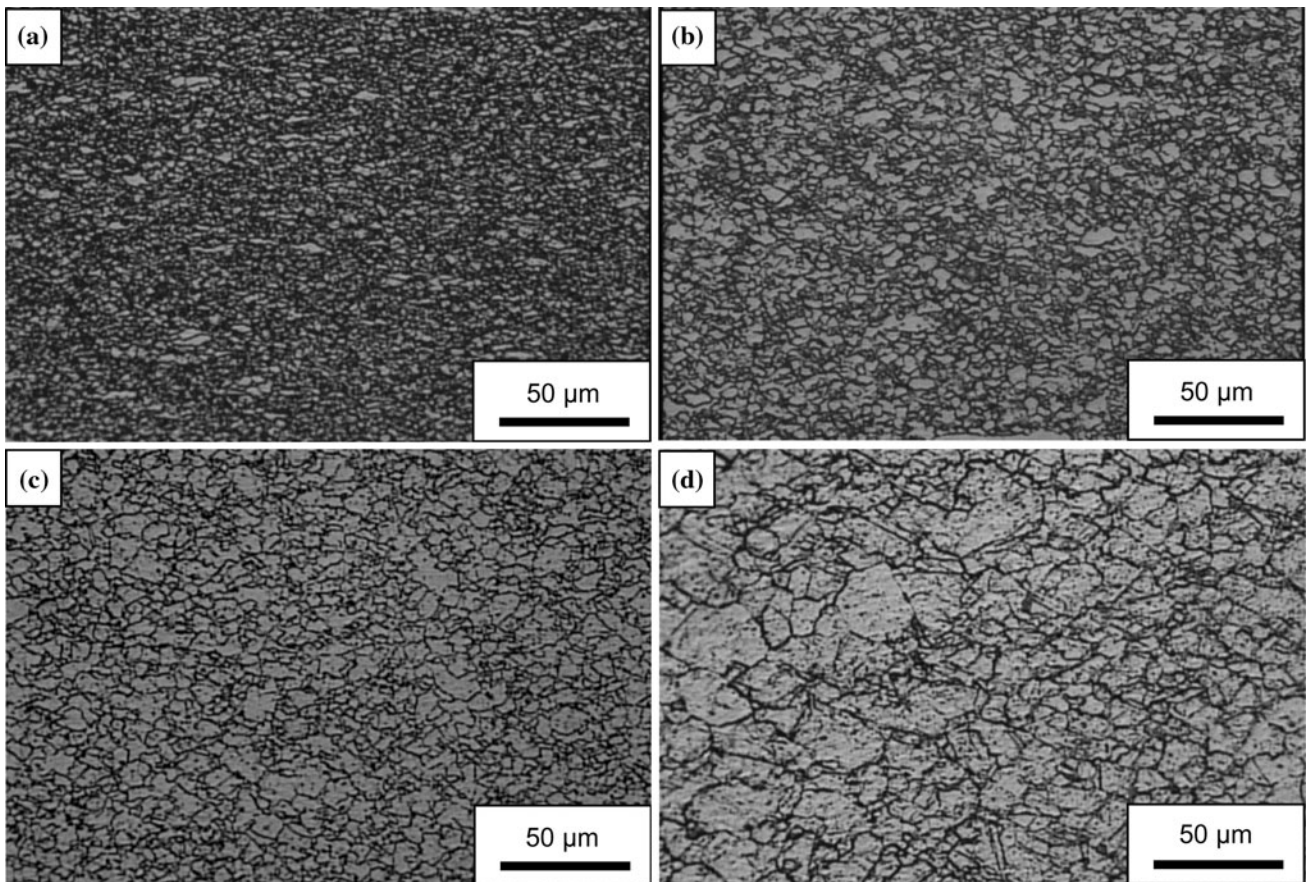
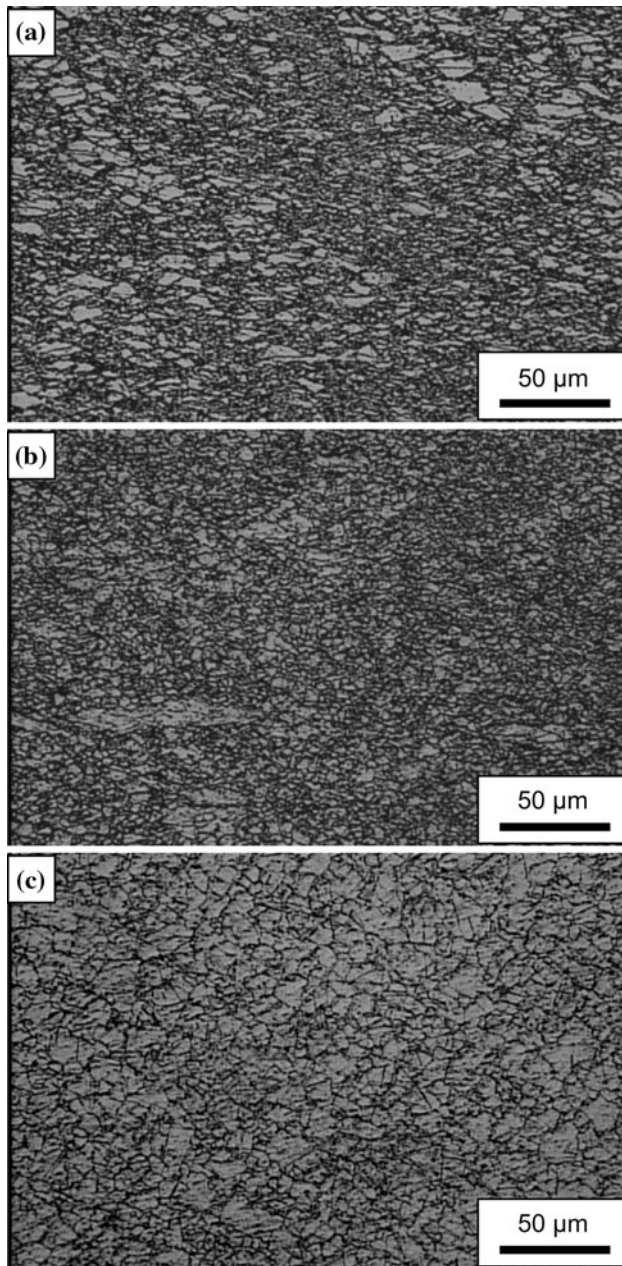
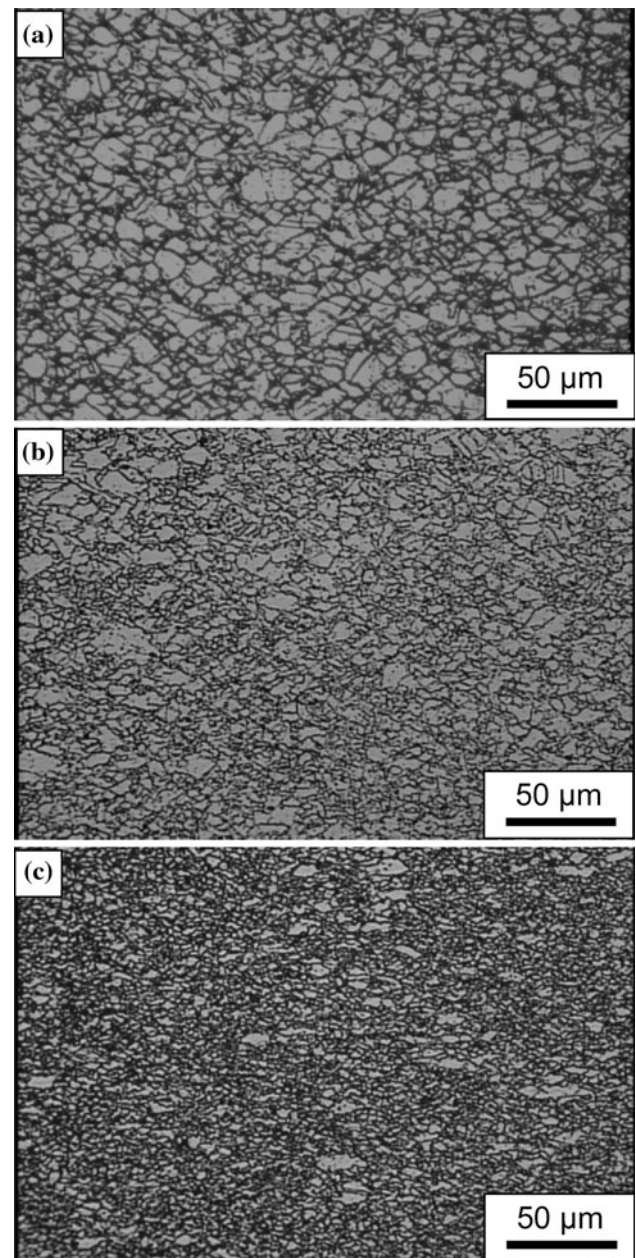


Fig. 8 Optical microstructures of the hot compressed IN 600 specimens under different deformation conditions at **a** 900 °C and 10 s^{-1} , **b** 950 °C and 1 s^{-1} , **c** 1050 °C and $1 \times 10^{-1} \text{ s}^{-1}$, and **d** 1100 °C and $1 \times 10^{-2} \text{ s}^{-1}$

Table 2 $\ln Z$ values based on the peak stresses for the IN 600 specimens under different deformation conditions (s^{-1})

	$1 \times 10^{-3} s^{-1}$	$1 \times 10^{-2} s^{-1}$	$1 \times 10^{-1} s^{-1}$	$1 s^{-1}$	$10 s^{-1}$
900 °C	26.94	29.24	31.55	33.85	36.15
950 °C	25.56	27.86	30.16	32.46	34.77
1000 °C	24.28	26.58	28.89	31.19	33.49
1050 °C	23.10	25.41	27.71	30.01	32.31
1100 °C	22.01	24.31	26.61	28.92	31.22
1150 °C	20.99	23.30	25.60	27.90	30.20

**Fig. 9** Microstructures of the specimens tested under different conditions with similar Z values at **a** 950 °C and $10^{-1} s^{-1}$ ($Z = 30.16$), **b** 1050 °C and $1 s^{-1}$ ($Z = 30.01$), and **c** 1150 °C and $10 s^{-1}$ ($Z = 30.20$)**Fig. 10** Microstructural evolution tested at 900 °C and a strain rate of $1 \times 10^{-1} s^{-1}$ at **a** $\varepsilon = 0.2$, **b** $\varepsilon = 0.4$, and **c** $\varepsilon = 0.6$

The microstructures under the deformation conditions with similar Z values are given in Fig. 9. Figure 9a shows that a lower degree of DRX was observed at a lower temperature with a lower strain rate. The degree of DRX should decrease at lower temperatures because of lower diffusivity. The decrease in strain rate could provide more time for diffusion to take place, which should increase the degree of DRX. Hence, a lower degree of DRX observed at

a lower temperature with a lower strain rate indicates that temperature has higher effect than strain rate on the degree of DRX under the deformation conditions with similar Z values. Figure 9c shows that a larger grain size was found on testing at a higher temperature with a higher strain rate. The DRX kinetics increases with increasing temperature, which should result in an increase in the size of DRX grains. However, the increase in strain rate

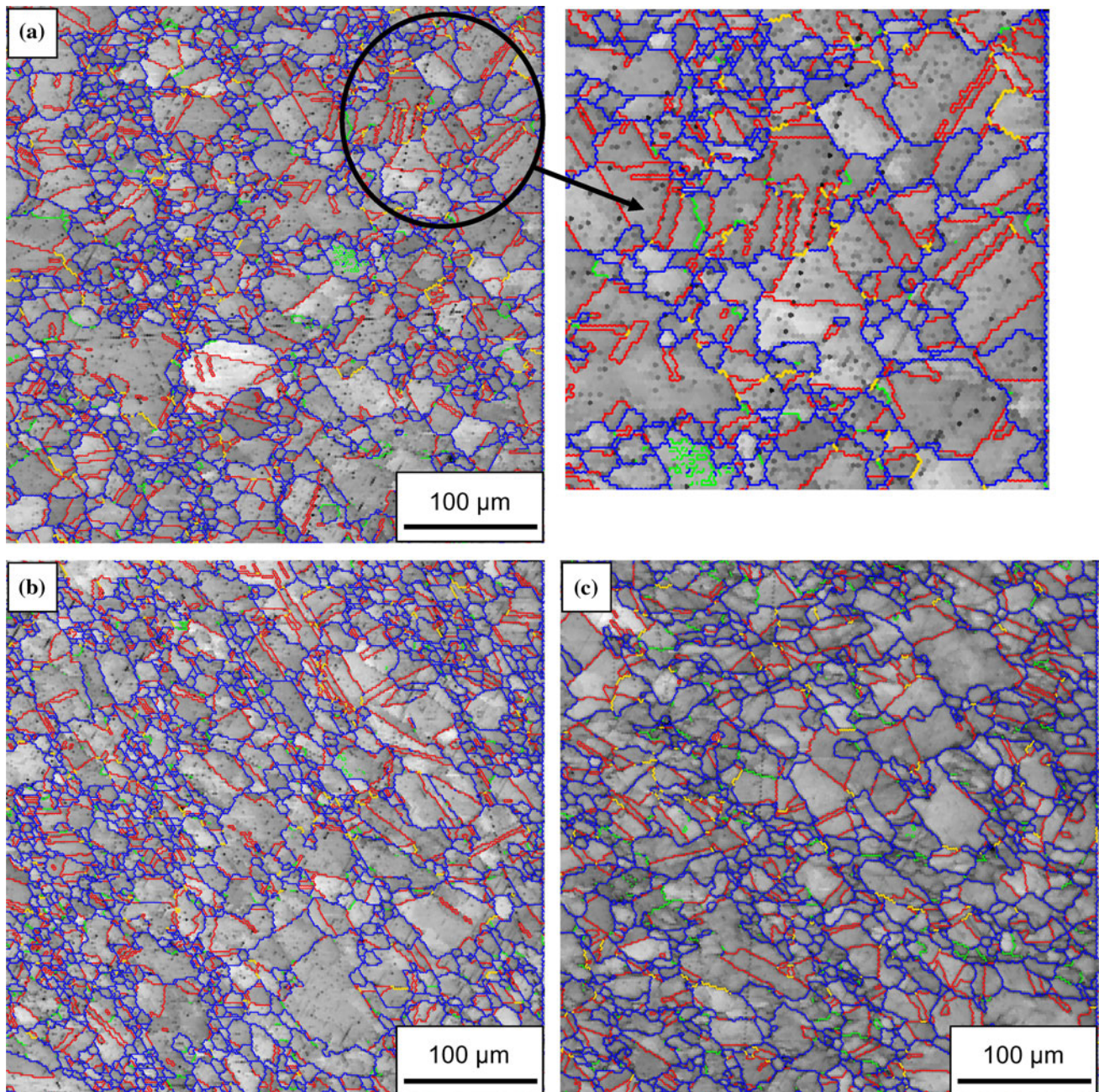


Fig. 11 Microstructural evolution analyzed by EBSD tested at 1050 °C and a strain rate of $1 \times 10^{-3} \text{ s}^{-1}$ at **a** $\varepsilon = 0.2$, **b** $\varepsilon = 0.4$, and **c** $\varepsilon = 0.6$ (green = 5°–15° low angle grain boundary,

blue = 15°–62.8° high angle grain boundary, red = $\langle 111 \rangle$ 60° twin grain boundary, yellow = $\langle 110 \rangle$ 38.9° twin grain boundary) (Color figure online)

Fig. 12 Grain size distribution analyzed by EBSD at various strains tested at 1050 °C and a strain rate of $1 \times 10^{-3} \text{ s}^{-1}$. **a** Original, **b** at $\varepsilon = 0.2$, **c** at $\varepsilon = 0.4$, and **d** at $\varepsilon = 0.6$

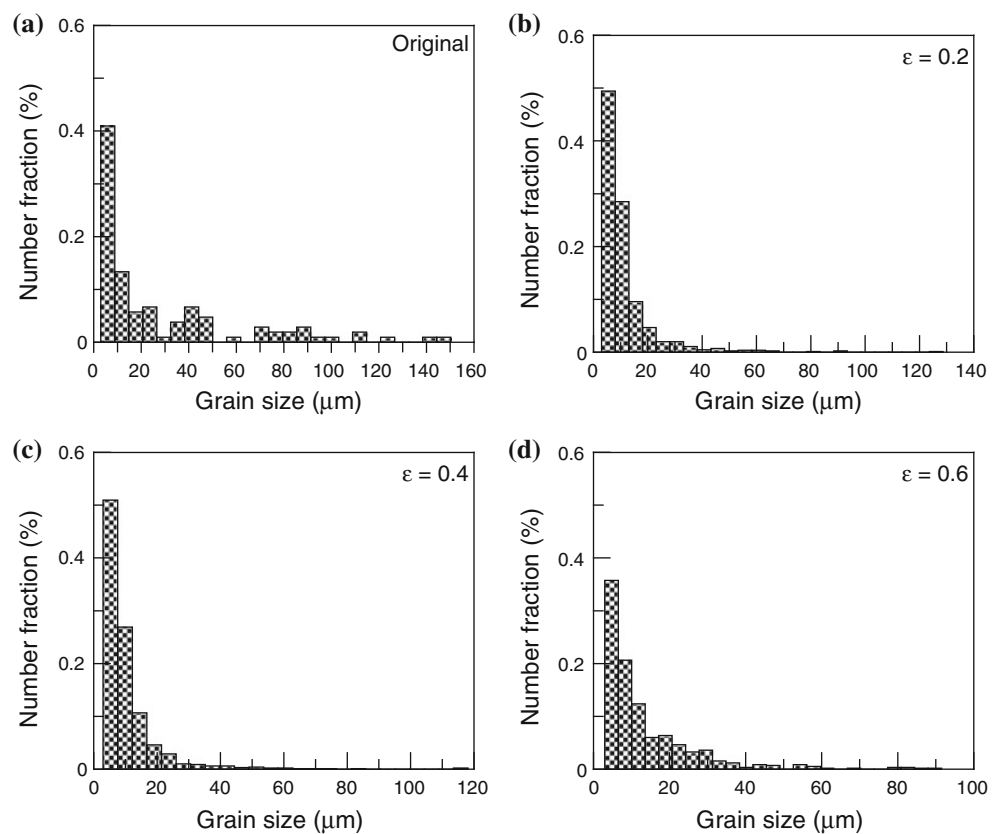


Table 3 n values obtained from stress–strain data at various strains for IN 600

Strain	0.2	0.3	0.4	0.5	0.6	0.7
n value	4.72 ± 0.14	4.59 ± 0.23	4.51 ± 0.22	4.49 ± 0.22	4.60 ± 0.23	4.78 ± 0.21

corresponds to a decrease in the DRX kinetics, which should lead to a decrease in the size of DRX grains. Therefore, a larger grain size observed at a higher temperature with a higher strain rate also shows that temperature has higher influence than strain rate on the recrystallized grain size under the deformation conditions with similar Z values.

Figure 10 shows the microstructural evolution tested at 900 °C and at a strain rate of $1 \times 10^{-1} \text{ s}^{-1}$ ($Z = 33.85$), indicating the degree of DRX increases with increasing strain. DRX is the major softening effect in the flow behavior tested at a high Z value. The increase in the degree of DRX with strain results in continuously decreasing flow stress in the flow curve after reaching the peak stress (Fig. 2a).

The EBSD microstructures at various strains on testing at 1050 °C and at a strain rate of $1 \times 10^{-3} \text{ s}^{-1}$ ($Z = 23.10$) are given in Fig. 11. Grain size distributions at various strains analyzed by EBSD are given in Fig. 12. Figure 11 shows that the microstructural evolution at a low Z value is different from that at a high Z value. Figure 12

shows that the number fraction for the smallest grain size ($\sim 5 \mu\text{m}$) increases with increasing strain, reaches a maximum value at a strain of approximately 0.4, and then decreases. Decreases in the number fractions of the grains with small sizes and increases in the number fractions of the grains with large sizes at a strain of 0.6 reveal the occurrence of grain growth of the dynamically recrystallized grains (Fig. 12d). These results indicate that DRX is the dominant softening effect at low strains, whereas growth of the dynamically recrystallized grains is responsible for softening at high strains. Figure 11 shows that the more important microstructural feature is twinning. The shape of the twins reveals that most of the twins are annealing twins. Mechanical twins tend to be lens shaped with sharp edges since this reduces the long range elastic strains. Annealing twins are not pointed because there are formed as a consequence of growth accidents during recrystallization of deformed cubic-close packed metals such as copper, austenitic iron, and nickel [27–29]. The microstructure observations indicate that strain influences

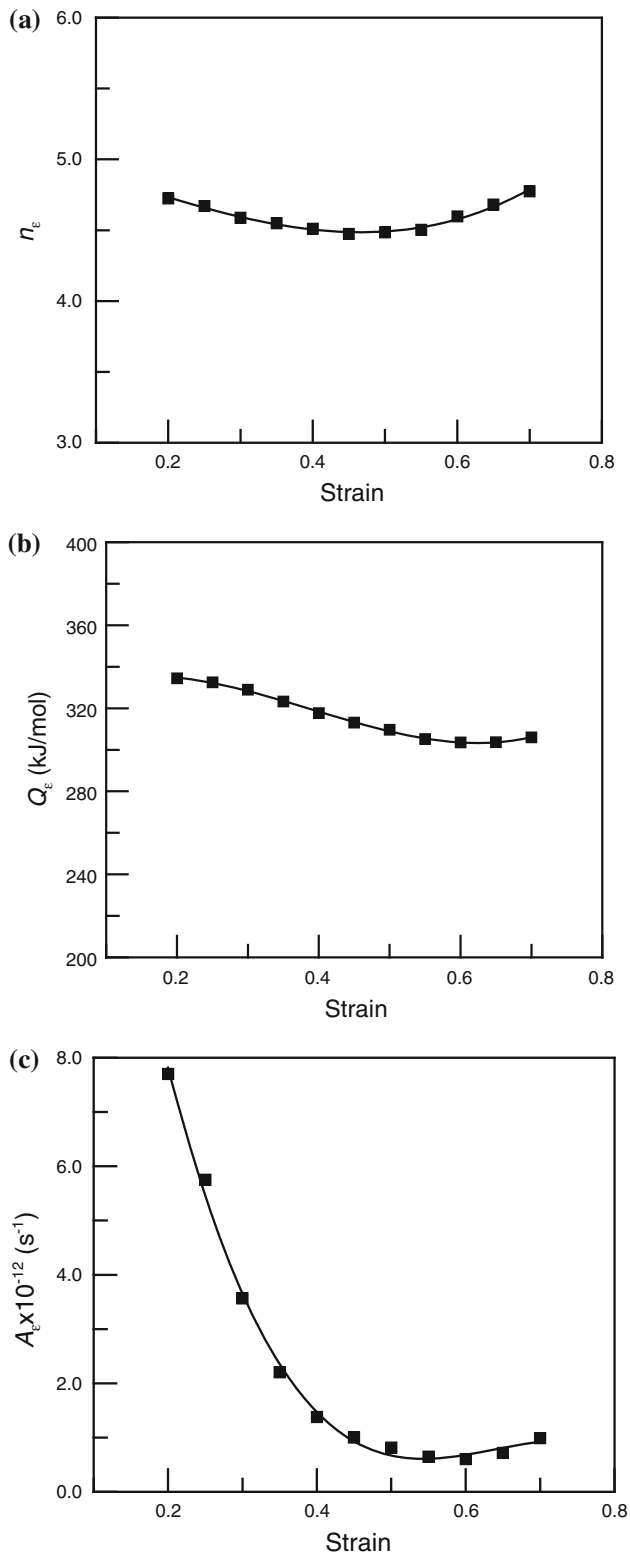


Fig. 13 Variations in constitutive parameters as a function of strain. **a** n value, **b** Q value, and **c** A value

the microstructural changes. Changes in the microstructure also affect the deformation mechanism, consequently influencing the constitutive analysis.

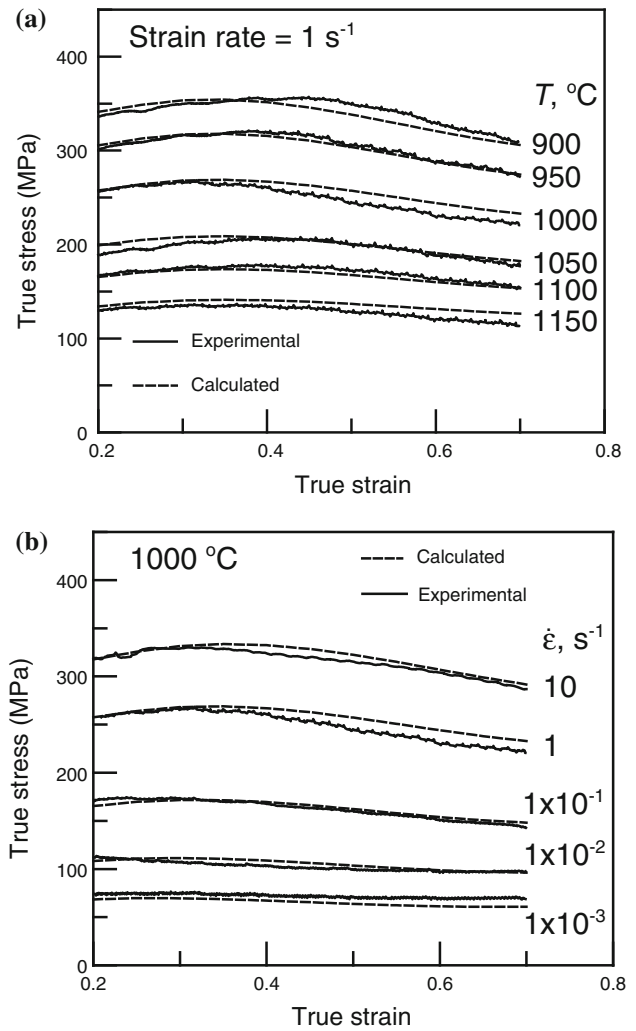


Fig. 14 Measured and calculated flow stresses of IN 600 **a** at a strain rate of 1 s^{-1} and various temperatures and **b** at $1000 \text{ }^\circ\text{C}$ and various strain rates

Strain-dependent constitutive analysis

The most important use of a constitutive equation is to calculate the flow stresses during hot working. The constitutive parameters are often calculated for peak or steady state stresses, because many models assume that plastic flow occurs with constant flow stress. However, the flow stress may be strain-dependent during hot deformation [17, 30–33]; thus, calculating the flow stress using constitutive equation with strain incorporated is necessary. Verlinden et al. [32] developed a generalized constitutive equation for an AA6060 aluminum alloy and showed that the hyperbolic sine constitutive equation could be used to calculate the flow stress at any strain, with constant values for the parameters A , n , and Q , and a strain-dependent α value. However, this study does not exhibit similar results for IN 600. Table 3 tabulates the stress exponent n values

obtained using Eq. 2 at various strains with a single α value of 0.005 MPa^{-1} . The maximum standard deviations for n values at various strains are all less than 5%. These results indicate that parallel lines can be obtained from the plots of $\ln \dot{\epsilon}$ versus $\ln[\sinh(\alpha\sigma)]$ at various strains using a single α value for IN 600. Hence, α value is treated as constant in this study.

Figure 13 shows the values of n , Q , and A as a function of strain. The decreases in the n , Q , and A values at low strains are consistent with the flow behavior, in which the flow stresses increase in this region. At high strains, the Q value remains constant, whereas the n and A values increase again. The variations in constitutive parameters with strain can be related to the stress–strain behavior. As shown in Fig. 2, most of the flow curves show decreasing flow stress after reaching the peak value. Therefore, the increases in the n and A values at large strains on testing at a given strain rate and temperature compensate for the decline of flow stress in response to dynamic softening.

Although Fig. 13a, b shows that the variations in n and Q values are not significantly sensitive to the strain, they cannot be treated as constants. If n and Q values are treated as constants at a given strain rate and temperature, Eq. 1 indicates that the variations in flow stress at different strains will follow the changes in A value under all test conditions. However, these are not the flow behaviors observed in the stress–strain curves (Fig. 2). Figures 10 and 11 also show that changes in the microstructures, which influence the deformation mechanisms, are strain-dependent. Consequently, the constitutive parameters are strain-dependent. Based on the data shown in Fig. 13, polynomial fittings are used to correlate the constitutive parameters with strains in this study. Hence, the strain-dependent constitutive equation for IN 600 can be expressed as follows:

$$\dot{\epsilon} = A_{\epsilon} [\sinh(0.005\sigma_{\epsilon})]^{n_{\epsilon}} \exp\left[\frac{Q_{\epsilon}}{RT}\right] \quad (6)$$

with $A_{\epsilon} = (24.38 - 116.04\epsilon + 185.57\epsilon^2 - 96.66\epsilon^3) \times 10^{12} \text{ s}^{-1}$, $n_{\epsilon} = 5.06 - 1.58\epsilon - 1.20\epsilon^2 + 4.14\epsilon^3$, and $Q_{\epsilon} = 322.2 + 185.5\epsilon - 740.64\epsilon^2 + 632.4\epsilon^3$.

A comparison of some experimental stress–strain curves and the stress values calculated using Eq. 6 is given in Fig. 14. The figure shows that the calculated flow stress values are in close agreement with the experimental flow curves.

Conclusions

The hot deformation behavior of an IN 600 superalloy was investigated in compression at 900–1150 °C, with strain rates ranging from 1×10^{-3} to 10 s^{-1} . The flow stress

varied not only with the strain rate and temperature but also with strain. The peak stress did not significantly increase with decreasing temperature at low strain rates. In contrast, the differences in the peak stresses between different temperatures were much greater at high strain rates. Flow behavior was associated with the microstructural evolution during hot deformation. Microstructure observations showed that the degree of DRX increased with increasing strain at a high Z value, resulting in a decline in the flow stress after reaching the peak stress. Constitutive analysis indicates that the hot deformation behavior of the IN 600 superalloy satisfied the hyperbolic sine constitutive equation. When the stress multiplier α in the hyperbolic sine equation was kept unchanged while the other parameters were made to be strain-dependent, the constitutive equation obtained could be used to calculate flow stress at any strain.

Acknowledgements This study was financially supported by the Nanopowder and Thin Film Technology Center, ITRI South, Industrial Technology Research Institute.

References

- McQueen HJ, Imbert CAC (2004) *J Alloys Compd* 378:35
- Fang YL, Liu ZY, Song HM, Jiang LZ (2009) *Mater Sci Eng A* A526:128
- Guo SL, Li DF, Pen HJ, Guo QM, Hu J (2011) *J Nucl Mater* 410:52
- Semiatin SL, Fagin PN, Glavicic MG, Raabe D (2004) *Scripta Mater* 50:625
- Medeiros SC, Prasad YVRK, Frazier WG, Srinivasan R (2000) *Mater Sci Eng A* A293:198
- Ponge D, Gottstein G (1998) *Acta Mater* 46:69
- Sellars C, Tegart WM (1966) *Acta Metall* 14:1136
- Sellars C, Tegart WM (1972) *Int Metall Rev* 17:1
- McQueen HJ, Ryan ND (2002) *Mater Sci Eng A* A322:43
- Hsu SE, Edwards GR, Sherby OD (1983) *Acta Metall* 31:763
- Cai DY, Xiong LY, Liu WC, Sun GD, Yao M (2009) *Mater Des* 30:921
- Yuan H, Liu WC (2005) *Mater Sci Eng A* A408:281
- Thomas A, El-Wahabi M, Cabrera JM, Prado JM (2006) *J Mater Process Technol* 177:469
- Jiang P, Fu WT, Wang ZH, Bai XH, Zhao XC, Lv ZQ (2011) *J Mater Sci* 46:4654. doi:10.1007/s10853-011-5371-5
- Farnoush H, Momeni A, Dehghani K, Aghazadeh Mohandesi J, Keshmiri H (2010) *Mater Des* 31:220
- Slooff FA, Zhou J, Duszczyc J, Katgerman L (2008) *J Mater Sci* 43:7165. doi:10.1007/s10853-008-3014-2
- Luo J, Li MQ, Yu WX, Li H (2009) *Mater Sci Eng A* A504:90
- Lin YC, Liu G (2009) *Mater Sci Eng A* A523:139
- Bombač D, Fazarinc M, Kugler G, Spajić S (2008) *RMZ Mater Geovviron* 55:319
- Wang Y, Shao WZ, Zhen L, Yang L, Zhang XM (2008) *Mater Sci Eng A* A497:479
- Liu Y, Hu R, Li JS, Kou HC, Li HW, Chang H, Fu HZ (2009) *J Mater Process Technol* 209:4020
- Pruthi DD, Anand MS, Agarwala RP (1977) *J Nucl Mater* 6:206
- Prasad YVRK, Rao KP, Hort N, Kainer KU (2008) *Mater Lett* 62:4207

24. Zhang H, Konopleva EV, McQueen HJ (2001) *Mater Sci Eng A* 319–321:711
25. Zener C, Hollomon JH (1944) *J Appl Phys* 15:22
26. Dehghan-Manshadi A, Barnett MR, Hodgson PD (2008) *Mater Sci Eng A* A485:664
27. Rath BB, Imam MA, Pande CS (2000) *Mater Phys Mech* 1:61
28. Pande CS, Ashraf Imam M (2009) *Mater Sci Eng A* A512:82
29. Mahajan S, Pande CS, Imam MA, Rath BB (1997) *Acta Mater* 45:2633
30. Slooff FA, Zhou J, Duszczyc J, Katgerman L (2007) Constitutive behaviour of wrought magnesium alloy AZ61. In: Beals RS, Luo AA, Neelameggham NR, Pekguleryuz MO (eds) *Magnesium Technology 2007*. TMS, Warrendale, p 363
31. Slooff FA, Zhou J, Duszczyc J, Katgerman L (2007) *Scripta Mater* 57:759
32. Verlinden B, Suhadi A, Delaey L (1993) *Scripta Metall* 28:1441
33. Momeni A, Dehghani K (2011) *Mater Sci Eng A* A528:1448